Clim Dyn (2016) 47:2105–2119
DOI 10.1007/s00382-015-2953-y

Active AMOC–NAO coupling in the IPSL-CM5A-MR climate model

Na Wen[1,2] · **Claude Frankignoul**[2] · **Guillaume Gastineau**[2]

Received: 24 March 2015 / Accepted: 13 December 2015 / Published online: 22 December 2015

Abstract The atmospheric response to the AMOC variability is investigated in the IPSL-CM5A medium resolution climate model, using lagged maximum covariance analysis (MCA) of a control simulation. A robust atmospheric response is detected in winter, with a negative NAO-like response following by about 9-year an AMOC intensification in the North Atlantic, with a pattern broadly resembling the second mode of AMOC variability. The response is established through the SST footprint of the AMOC and the associated surface heat flux damping, with a dipole of SST anomalies made of cold SST in the Gulf Stream region and warm SST further northeast around the North Atlantic Current. The dipole SST anomaly pattern evolves synchronously with the AMOC changes at its dominant 20-year period, so that the lagged NAO-like response detected by MCA actually reflects the near-synchronous AMOC influence on the atmosphere, which is masked at short time lag by the stronger atmospheric forcing of the AMOC. The atmospheric response to an intensification of the AMOC is thus a positive NAO-like pattern, together with an anomalous low pressure over the Aleutians, opposite to that detected at 9-year lag by the MCA. Since the NAO also contributes to force the AMOC, there is a positive feedback between AMOC and NAO in the model, with the atmospheric feedback strength about 1/4 of that of the atmospheric forcing, which enhances the low frequency variability of AMOC. This is further confirmed by the lead-lag relation between the dominant mode of ocean and atmosphere, and by the robust 20-year period of the NAO.

Keywords AMOC · NAO · Atlantic multi-decadal variability · Air–sea interaction · Climate models

1 Introduction

Climate models (e.g., Frankcombe et al. 2010) and observations (Rayner et al. 2011) show that the natural variability of the Atlantic meridional overturning circulation (AMOC) induces substantial changes in the meridional oceanic heat transport, and may thus significantly contribute to the low frequency climate variability. It has been suggested that the AMOC influences the observed multidecadal sea surface temperature (SST) variability in the North Atlantic, which is often called the Atlantic Multidecadal Oscillation (AMO; Latif et al. 2004; Vellinga and Wu 2004; Knight et al. 2005; Mignot et al. 2007). The AMO has some well-established impact on the climate in the regions surrounding the North Atlantic, such as the North America and European climate or the summer rainfall over Sahel or North-eastern Brazil (Rodwell et al. 1995; Sutton and Hodson 2005; Pohlmann et al. 2006; Hodson et al. 2010). However, the variability of AMO is not only due to the AMOC change, as it is also affected by the external forcings (Ottera et al. 2010; Booth et al. 2012; Marini and Frankignoul 2013), and the natural variability of the atmosphere (Ting et al. 2014; Gastineau and Frankignoul 2015). Lacking long term ocean records, it is difficult to establish a clear relation between the AMOC, SST and the atmosphere in observations. Therefore, despite their shortcomings, climate model provides the best way to investigate the AMOC variability and its climate influence.

✉ Na Wen
wenna@nuist.edu.cn

[1] Key Laboratory of Meteorological Disaster of Ministry of Education and College of Atmospheric Sciences, Nanjing University of Information Science and Technology, Nanjing 210044, China

[2] CNRS/IRD/MNHN, LOCEAN/IPSL, Sorbonne Universités (UPMC, Univ. Paris 06), Paris, France

Most climate models exhibit a pronounced decadal or multidecadal variability of the AMOC, but the dominant mechanisms responsible for this variability vary substantially from model to model (Frankcombe et al. 2008; Liu 2012; MacMartin et al. 2013). In some models, the AMOC variability primarily reflects the stochastic atmospheric forcing with the ocean setting the time scale (Delworth and Greatbatch 2000; Dong and Sutton 2005; Jungclaus et al. 2005; Kwon and Frankignoul 2014). However, others suggest that two-way ocean–atmospheric interactions play a dominant role (Timmermann et al. 1998; Farneti and Vallis 2009). However, the atmospheric response to the AMOC variability appears to be weak, and varies among the climate models. Msadek and Frankignoul (2009) found a weak positive feedback between the East Atlantic pattern and the AMOC in an early version of the IPSL-CM4 model, while Gastineau and Frankignoul (2012, hereafter GF12) detected an AMOC influence on the cold season atmosphere in six climate models, with an enhanced AMOC followed by a negative NAO response after 4–9 years, depending on the model. Yet, Frankignoul et al. (2013) found in CCSM3 a significant positive NAO response (3-year lag) to an AMOC intensification in the red noise regime, but hints a negative NAO response in the oscillatory regime.

Estimating the atmospheric influence of the AMOC is difficult because the large atmospheric internal variability leads to a small signal-to-noise ratio (Teng et al. 2011). The atmospheric response to the AMOC depends on the AMOC-induced SST and surface heat flux anomaly, but the latter may be time-dependent so that the lag at which a significant response is detected depends on the evolution of the AMOC fingerprint (GF12). However, if the response is detected at a lag of about one half of the dominant AMOC period in climate models with a marked oscillatory behavior, it may be that it actually reflects a faster response of the opposite sign that is masked at short lags by the atmospheric forcing of the AMOC. Here we suggest that this is a case in the IPSL-CM5A-MR climate model (Dufresne et al. 2013).

The purposes of the paper are in the following: (1) to evaluate the AMOC influence on the atmosphere using the IPSL-CM5A-MR model; (2) to understand how the atmospheric responds to the AMOC variability through the AMOC-induced SST anomaly. The results indicate an active AMOC influence on the NAO, via its dipolar SST footprint centered over the Gulf Stream/North Atlantic Current region. It is found that the negative NAO-like-pattern detected when an AMOC amplification leads by about 9 years actually reflects the near-instantaneous AMOC influence on the atmosphere, with an enhanced AMOC driving a positive NAO-like response, which suggests a positive feedback between AMOC and NAO, and an active coupling on the 20-year period. The rest of the paper is arranged as follows. Section 2 describes the model and the statistical method. In Sect. 3, the ocean feedback signal is shown, and the relations between the AMOC, SST and the atmosphere are discussed. The mechanism of the interaction between AMOC and NAO is investigated in Sect. 4. The last section gives the summary and discussion.

2 Model and methods

2.1 Model

The IPSL-CM5A-MR climate model (hereafter IPSL-MR), where MR stands for medium resolution, consists of the LMDZ5A atmospheric model, the NEMO ocean model (which includes the OPA9 ocean circulation model, the LIM-2 sea-ice model and the PISCES oceanic biogeochemistry model), and the ORCHIDEE land surface model, coupled with the OASIS3 module (Dufresne et al. 2013). The atmospheric model has 39 vertical levels and the horizontal resolution of 2.5° (in longitude) and 1.25° (in latitude), instead of 3.75° and 1.87° for the low resolution (LR) version of the same IPSL-CM5A model, hereafter IPSL-LR. The ocean model uses the ORCA2 configuration, with an irregular grid using a nominal resolution of 2° increasing to 0.5° over tropical regions and the Arctic, and 31 vertical levels with increased resolution in the upper 150 m. In this study, the last 300 years of the 500-year control run are considered, after a spin-up of 200 years. To remove the remaining drift, all the model data are detrended by a third-order polynomial before the analysis.

IPSL-MR is a version of the IPSL-CM5A model using a better resolution, which improves the climate simulation, especially in midlatitudes. In particular, the location of the jet stream and the storm tracks is more realistic (Barnes and Polvani 2013; Arakelian and Codron 2012), which reduce the cold bias over mid-latitudes (Dufresne et al. 2013). Therefore, the sea ice cover in the Labrador and Nordic Seas is slightly reduced, and more convection occurs in the Southern Labrador Sea (not shown). Nevertheless, a cold bias remains over the North Atlantic region, with excessive sea ice cover. As shown in Fig. 1a, the mean AMOC, as diagnosed by the meridional streamfunction within the Atlantic Ocean, reflects the northward mass flux in the upper ocean, sinking between 45° and 60°N, and the southward return flow of North Atlantic Deep Water (NADW). Its maximum value is 13 Sv near 35N and 1000 m depth, which is a larger than the 10 Sv of IPSL-LR (GF12), but remains underestimated compared with the observations (Ganachaud and Wunsch 2003; McCarthy et al. 2012) or ocean model hindcast simulations (Yeager and Danabasoglu 2014). Note also that the Antarctic Bottom Water cell below 2000 m extends too far north.

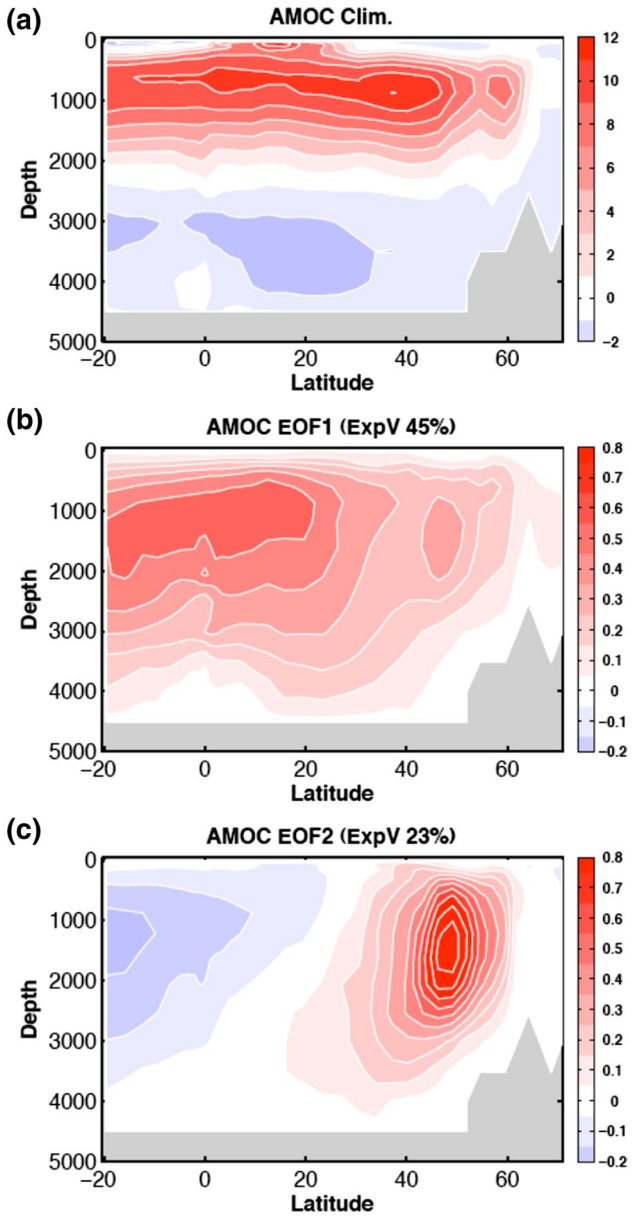

Fig. 1 **a** Mean meridional overturning streamfunction in the Atlantic Ocean (in Sv) for the last 300-year control run data in IPSL-CM5A-MR model. Contour interval (CI) is 2 Sv with positive (negative) for clockwise (counterclockwisec) circulation. **b** First and **c** second leading EOF mode of the meridional overturning streamfunction (CI = 0.1 Sv) with explained variance 45 and 23 % respectively. Here, the EOF amplitude corresponds to a normalized PC with unit variance

The dominant modes of the yearly AMOC in the MR model are presented in Fig. 1b, c. The first leading Empirical Orthogonal Function (EOF) of the meridional overturning streamfunction (Fig. 1b) exhibits a basin scale monopole circulation anomaly with a broad maximum in the tropical Atlantic at 1500 m depth. It indicates the acceleration (deceleration) and deepening (shallowing) of the AMOC, most importantly between 20°S and 20°N. This mode explains 45 % of the variance and has a dominant time scale 50–70 years (not shown). The second EOF mode (EOF2, Fig. 1c) shows a dipole pattern with a dominant circulation anomaly taking place mostly between 20N and 60N and a weaker anomaly of the opposite sign south of 20N. Although it only explains 23 % of the variance, the EOF2 mainly dominates the AMOC variability in the North Atlantic from 35°N to 60°N, with a dominant period of 20 years (as illustrated in Sect. 3 and Fig. 10). Note that the EOF1 pattern is specific to IPSL-MR and that EOF2 broadly resembles EOF1 in IPSL-LR, but for its opposite in sign south of 35°N (see Fig. 2 in GF12).

2.2 Statistical methods

2.2.1 Maximum covariance analysis

To investigate the atmospheric response to the AMOC variability as a function of season, we used a lagged MCA between the 3-month averaged sea level pressure (SLP) in the North Atlantic sector (10N–80N, 100W–40E) and yearly Atlantic meridional overturning streamfunction between 30S and 80N. Prior to the analysis, an elementary binomial filter, using ¼, ½, ¼ as weights, was applied to the yearly seasonal SLP and yearly AMOC time series, so that, for example, December–February at year n (DFJ_n) is replaced by $\frac{1}{4}DJF_{n-1} + \frac{1}{2}DJF_n + \frac{1}{4}DJF_n$, to highlight the low frequency without affecting seasonality. Hence, cause and effects are only fully separated when the ocean leads or lag by at least 3 years. The MCA is well documented (Bretherton et al. 1992; Czaja and Frankignoul 2002), and is only briefly summarized here. The lagged MCA isolates pairs of orthogonal spatial patterns (u_k, v_k) and their corresponding time series ($x_k(t), y_k(t-\tau)$) by performing singular value decomposition of the covariance matrix between SLP field $X(t)$ at time t and the Atlantic meridional overturning streamfunction $Y(t-\tau)$ at time $t-\tau$. The covariance between the time series $x_k(t)$ and $y_k(t-\tau)$ is maximized with $\mathrm{cov}(x_k, y_k) = \sigma_k$, where σ_k is the kth singular value of the covariance matrix. At each lag τ, the statistical significance of the squared covariance (SC) and correlation (R) between the time series $x_k(t)$ and $y_k(t-\tau)$ is assessed using a Monte Carlo approach, in which the atmospheric time series was randomly scrambled 100 times using 3-year blocks to build the null hypothesis distribution of the SC and correlation R. Note that in the MCA and EOF analysis, the SLP are area-weighted by the square root of the cosine of latitude and, for the AMOC, ocean layer thickness.

The spatial orthogonality of the MCA modes can be a strong constraint for physical modes (Cheng and Dunkerton 1995). To relax the constraint of the spatial orthogonality when displaying the atmospheric response to the

AMOC, the varimax rotation is performed by using the first four pairs of MCA modes, so that about 95 % of the SC is retained at the different lags. The results are basically insensitive to an increase of the number of the modes. To display the MCA results, we show the homogeneous maps for the ocean and heterogeneous maps for the atmosphere (obtained by projecting the oceanic and atmospheric anomaly data on the normalized oceanic time series, respectively) when the ocean leads, and conversely when the ocean lags. Thus, the linear relation between the variables is preserved in both cases (Czaja and Frankignoul 2002). In this study, we focus on the winter (DJF) atmospheric response to the yearly AMOC (centered on winter), as DJF provided the most robust relation between 3-month running mean SLP and the correspondingly centered yearly AMOC. When investigating the atmospheric response to the AMOC, the ENSO signal (as given by the first leading EOF mode of the tropical Pacific defined within 20S–20N, 100E–80W) is removed from both atmosphere and ocean as in Frankignoul and Kestenare (2002), using linear regressions. Note that similar results are obtained when the ENSO signal is not removed prior to analysis, as shown in Sect. 3.

2.2.2 *Equilibrium feedback assessment*

To assess the atmospheric response to a given SST anomaly pattern, we use the univariate method of Frankignoul et al. (1998), here named as equilibrium feedback assessment (EFA) for convenience. The philosophy of the method is that on the climate time scale, the atmospheric SLP variability $X(t)$ can be separated into two parts: one is driven by the SST anomaly $T(t)$, and the other is the atmospheric internal variability $N(t)$, such that

$$X(t) = b \times T(t) + N(t), \tag{1}$$

where the feedback coefficient b represents the atmospheric response to the SST anomaly forcing. Since the SST cannot be forced by later stochastic atmospheric fluctuations, the feedback coefficient b is derived as

$$b(\tau) = C_{XT}(\tau)C_{TT}^{-1}(\tau), \tag{2}$$

where $C_{XT}(\tau)$ represents the lagged covariance; $C_{TT}(\tau)$ is the SST autocovariance at lag τ where τ is a SST leading time that is larger than the atmospheric persistence and the atmospheric response time. Here the method is applied on monthly data, after removing the ENSO teleconnections, as previously illustrated. The leading time τ is taken as 2 months. Statistic significance of the coefficient b is estimated by the Monte Carlo approach, where the year of atmosphere variable is scrambled randomly 1000 times with the month sequence retained.

3 Atmospheric response to the AMOC variability

3.1 MCA analysis

Figure 2 shows the square covariance (SC) and correlation (R) of the first MCA mode with (black line) and without (blue line) ENSO. The large similarity between the two curves indicates little influence of ENSO on the relation between the North Atlantic atmosphere and the AMOC. Nonetheless, the ENSO signal is removed in the following. When the atmosphere leads, there is a large and significant peak in the SC (which is the primary quantity to be considered as it is maximized) at lag 1 and 2, and a smaller but still highly significant one around lag 12–13. This reflects the atmospheric forcing of the AMOC. The correlation is also highly significant, but it peaks at lag 0, possibly reflecting sampling uncertainties. Figure 3 shows the atmospheric forcing and its corresponding AMOC response patterns, as given by the MCA at lag 1 and 12 respectively. When atmosphere leads by 1 year, the atmospheric anomaly resembles the North Atlantic oscillation (NAO) with a positive pressure anomaly over the Azores and a negative anomaly over the Arctic (Fig. 3b). It leads an enhanced AMOC in the North Atlantic with a monopole cyclonic overturning circulation anomaly centered between 45N and 50N (Fig. 3a), which resembles the AMOC EOF2 in Fig. 1c, except that it is shifted slightly southward. The previous studies (Eden and Willebrand 2001; Deshayes and Frankignoul 2008) indicate that the AMOC response to the NAO consist of a fast (on seasonal scale) barotropic adjustment and a slower, more persistent baroclinic reponse. Here, the difference between Fig. 3a and the AMOC EOF2 might be due to the smoothing that mixes the fast barotropic and the delayed baroclinic responses of the AMOC (see Fig. 11 below). The response amplitude is around 0.5 Sv for a change of the SLP of 300 Pa, at the center of actions of the NAO. When the atmosphere leads by 12 years (Fig. 3c, d), the MCA shows that a NAO patterns precedes a slightly weakened AMOC amplitude, which a pattern again resembling AMOC EOF2, but with the opposite phase, showing a weaker counterclockwise circulation located somewhat further north. This weakened AMOC response at lag 12 reflects the 20-year variability of AMOC EOF2.

A robust AMOC influence on the atmosphere is detected at negative lag, as there is a significant SC and R that peak around lag-9 (Fig. 2). When the ocean leads by 9 years, the first MCA mode is well separated and significant at the 95 % confidence level for both SC and R. The SC is a little smaller than at lag 12, which suggests that the AMOC influence on the atmosphere is smaller than the atmospheric forcing of the AMOC. Figure 4 shows the rotated

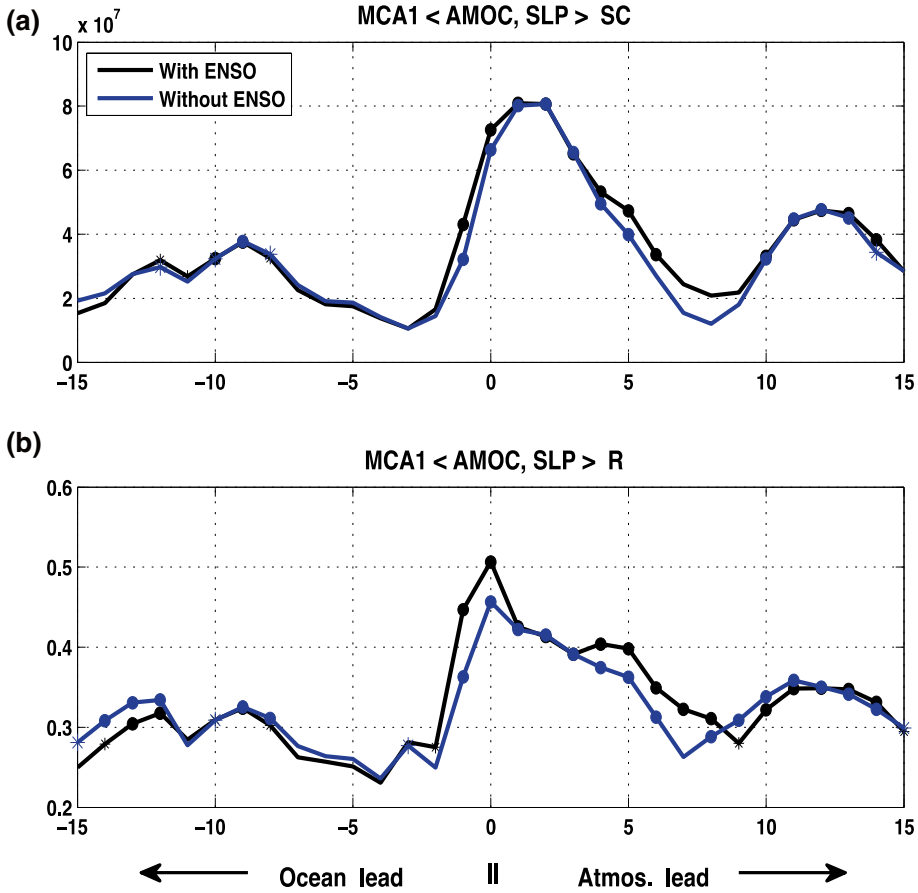

Fig. 2 **a** Squared covariance (unit: $Pa^2\ Sv^2$) and **b** correlation of the first MCA mode between the winter (DJF) SLP and yearly AMOC. The *black* and *blue lines* represent the MCA analysis with and without ENSO respectively. *Solid circle* (*star*) denotes the 95 % (90 %) confidence level. Lag is negative (positive) when AMOC (atmosphere) leads

MCA patterns. The AMOC forcing is a monopole cyclonic circulation anomaly in the northern North Atlantic with a maximum at 50°N (Fig. 4a) that again resembles the second EOF mode of AMOC, albeit without change of sign south of 20°N. The slight difference with AMOC EOF2, south of 20N, may be due to the MCA rotation relaxing the spatial orthogonal constraint, as the non-rotated MCA pattern shows more similarity with AMOC EOF2 (not shown). The corresponding AMOC time series (Fig. 5a) has a dominant period of 15–25 years, as shown by its power spectrum in Fig. 5b, which is highly correlated with the principle component of AMOC EOF2 around 0.83 in phase. The SLP response at lag-9 resembles a negative NAO pattern, albeit shifted eastward (Fig. 4b). The maximum response amplitude is typically about 100 Pa for the northern pole and −60 Pa for the southern pole, corresponding to about 30 % of the typical magnitude of the winter NAO. This suggests that the AMOC forcing contributes substantially to the NAO low-frequency variability.

The AMOC influence on the atmosphere is established through its SST and surface heat flux fingerprints. Figure 6 shows the regression maps of SST and surface heat flux lagged by 9 years onto the AMOC MCA time series at lag-9, so that they are in phase with the atmospheric response in Fig. 4b. Nine years after an enhanced AMOC, the SST anomalies are only significant in the North Atlantic, with little signal in rest of the global ocean (not shown), which indicates that the atmospheric response shown in Fig. 4b is mainly controlled by the North Atlantic air–sea interactions. The SST anomaly has a dipolar pattern with cooling in the Gulf Stream region and warming downstream around the North Atlantic Current. The typical amplitude of the anomalies is around 0.2–0.3 °C. There are also warm SST anomalies associated with the retreat of sea ice in the Nordic and Labrador Seas, but they are not 10 % significant. Accompanying the AMOC-induced SST anomaly, there is a large heat release from the ocean over the anomalously warm North Atlantic Current and a heat gain in the cold Gulf Stream region. This indicates that the ocean is forcing the atmosphere through the negative surface heat flux feedback, as in observations (Frankignoul and Kestenare 2002). However, the negative heat flux anomaly south of Greenland (ocean gaining heat) reflects the large-scale atmospheric response because the negative NAO-like signal weakens the westerly wind over this region. This is confirmed by the regression on the same AMOC index of the heat flux one season earlier in SON, when there is no significant large-scale response to the AMOC, which only

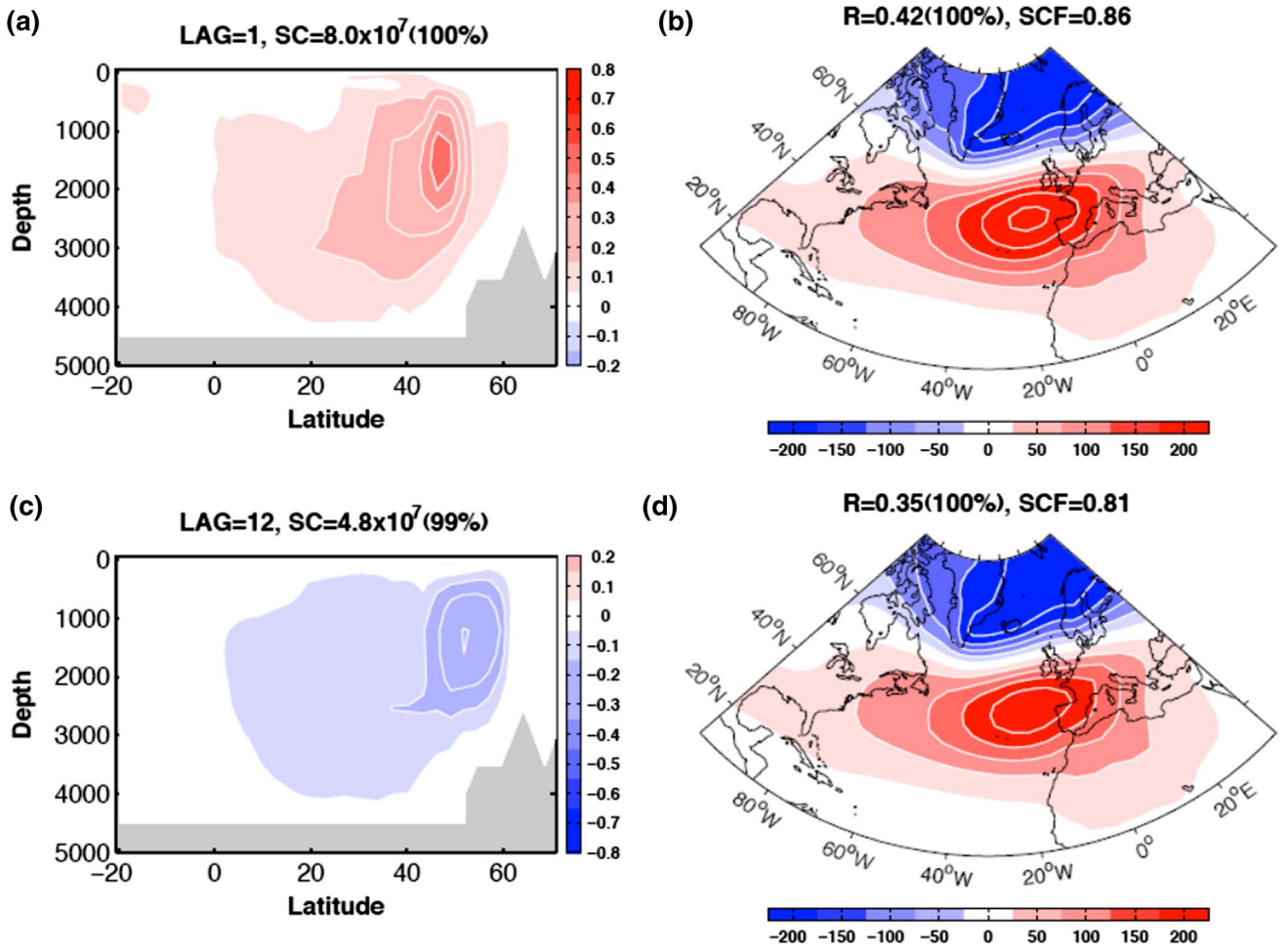

Fig. 3 Homogeneous map of the winter SLP (**b**, **d**) (CI = 50 Pa) and heterogeneous map of the yearly AMOC (**a**, **c**) (CI = 0.1 Sv with *red* for clockwise) for the first MCA mode, when atmosphere leads the ocean by 1 (*upper panels*) and 12 (*bottom panels*) years. SC is the square covariance in unit Pa^2 Sv^2, R is correlation and SCF is the SC fraction of the first MCA mode, with confidence level given in the *parentheses*

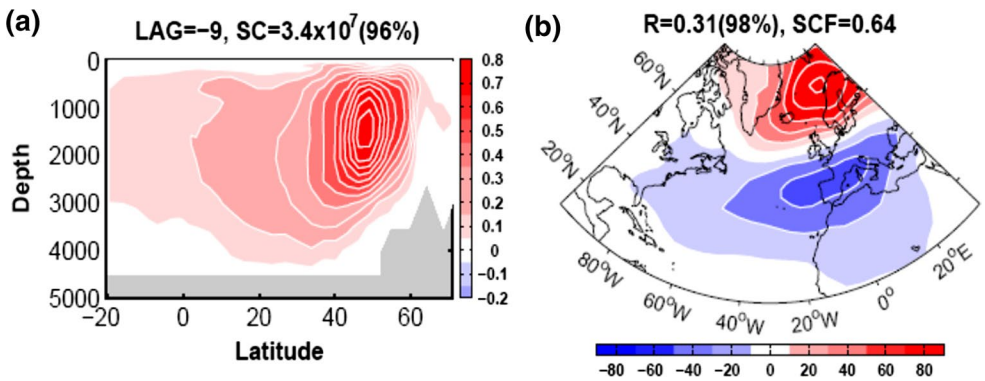

Fig. 4 Same as Fig. 3, but for the homogeneous map of the yearly AMOC (**a**) (CI = 0.1 Sv with *red* for clockwise) and heterogeneous map of the winter SLP (**b**) (CI = 20 Pa) for the first rotated MCA mode, when ocean leads the atmosphere by 9 years

shows the dipolar pattern of the SST and heat flux (not shown). Through the heat flux anomaly, the dipolar pattern SST affects the baroclinicity of the lower troposphere and thus the synoptic perturbation growth. The Eady growth rate at 850 hPa (Fig. 6c), defined as $0.31f|\partial u/\partial z|N^{-1}$, where f is the Coriolis parameter, $\partial u/\partial z$ is the zonal wind shear and N is the Brunt–Väisälä frequency, governs the amplitude of the fastest growing atmospheric perturbation (Hoskins and Valdes 1990). Consistent with the impact of the Gulf Stream cooling on the meridional SST gradient,

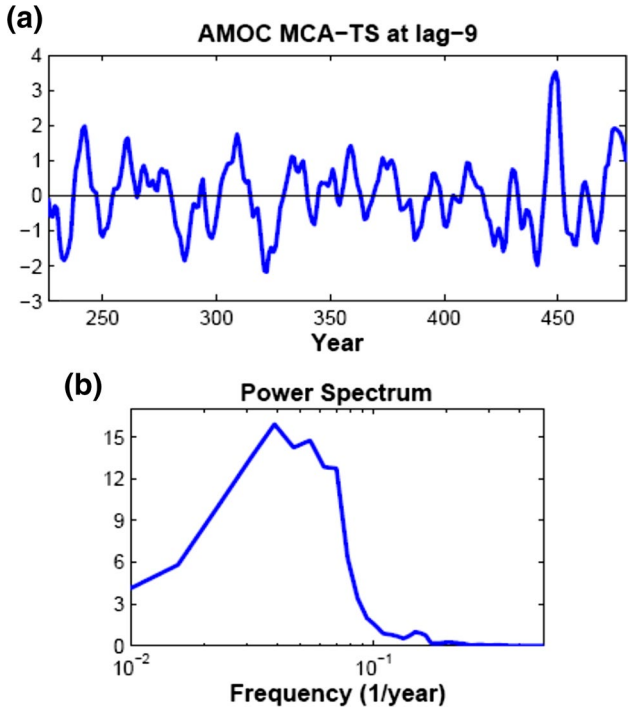

Fig. 5 **a** Normalized AMOC time series (*blue line*) of the first rotated MCA mode when AMOC leads by 9 years. **b** Power spectrum of the AMOC time series (*blue line* in *upper*) in variance preserving form

it shows reduced baroclinicity over and off Newfoundland, extending downstream toward Iceland, and a slight increase in baroclinicity in the subtropical North Atlantic, which results in a southward shift of the region of maximum synoptic growth. This decreases the storm track activity over the whole subpolar region, as shown by the standard deviation of the bandpass-filtered (2.2–6 days) 500 hPa geopotential height calculated from daily output (Fig. 6d). This is consistent with the negative NAO-like response in Fig. 4b.

An enhanced AMOC thus precedes a negative NAO-like signal by 9 years. However, this does not imply causality, as the AMOC variability is oscillatory, and the 9-year lag used to detect the response to the AMOC is close to half of its dominant period. Hence, it could be that the negative NAO-like response found at lag-9 reflects an in-phase response of the opposite sign. This is discussed in the next section.

3.2 Relationship between AMOC, SST and atmospheric response

The temporal evolution of the SST anomaly with the AMOC change is shown in Fig. 7. Between the AMOC intensification (defined by lag-9) and the atmospheric circulation changes 9 years later (designated as lag 0), which then correspond to an AMOC weakening (see Fig. 8), the SST anomaly pattern gradually reverses sign in the North Atlantic, evolving from a warm Gulf Stream and cold NAC into the opposite, albeit with a reduced amplitude, consistent with an oscillatory decay of the AMOC amplitude. The SST evolution pattern is similar to that of the heat content anomaly in the upper ocean 300 m, which is less affected by the weather noise and more sensitive to anomalous heat transport. Consistent with the geostrophic relation, an increased (decreased) AMOC corresponds to the density decreasing (increasing) eastward at 50°N, where the anomalous density is dominated by its salinity component (Fig. 7 middle-right panels). Figure 7 suggests that advective processes largely determine the evolution of the SST anomaly, in particular near 40°N–45°N, close to the mean Gulf Stream position in the model. When the AMOC weakens, the gyre circulation is decelerated, especially the subtropical gyre (right panels). Therefore, the northward heat transport is reduced and less warm water is advected in the Gulf Stream region, and vice versa when the AMOC strengthens. The process to form the SST anomaly at downstream of the North Atlantic Current is mainly related with the heat anomaly advected alone the North Atlantic Current and the subpolar gyre. Figure 7 (middle left) clearly shows that the positive heat content anomaly is advected in the subpolar gyre while the AMOC weakened, which is further confirmed by the eastward propagation of the meridional mean heat content anomaly in 50–55°N in Hovmöller plot (not shown). The evolution of the salinity in the upper ocean 300 m with the AMOC change (Fig. 7, middle right panel) indicates that a warm and salty water move along the North Atlantic Current, while another warm and salty water originating near the southern tip of Greenland is advected along the subpolar gyre. The two water masses eventually meet at the downstream of the North Atlantic Current. For the SST anomaly at the downstream of the North Atlantic, it might also involve other processes, such as the air–sea flux exchanges, overflow from the Nordic Sea and Rossby wave propagation at depth (Ortega et al. 2015). Hence, the relation of the upper ocean changes with the AMOC is roughly consistent with the previous studies (Eden and Willebrand 2001; Johns et al. 2011; Yeager et al. 2012) arguing that the boundary between the subtropical and subpolar gyre is a transition zone for the meridional heat transport, where the overturning circulation accounts for most of it to the south and the gyre circulation explains a large percent of the meridional heat transport to the north.

Since the atmosphere responds to SST anomaly within a few months at most (Deser et al. 2007), and the SST and AMOC patterns at lag-9 and 0 have opposite sign, it can be hypothesized that the lag relation in Fig. 4 simply reflects the atmospheric response to the in-phase SST fingerprint of the AMOC. This is supported by Fig. 8, which shows

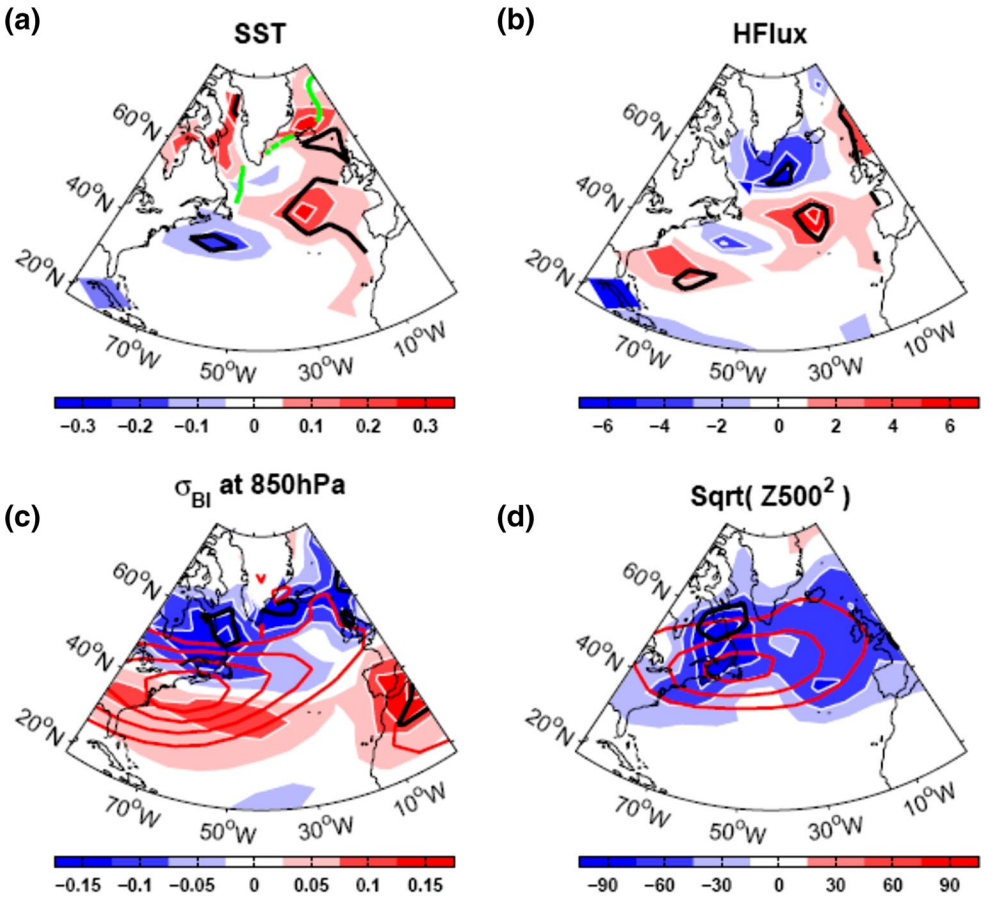

Fig. 6 Regression map of the winter **a** SST (in K), **b** surface heat flux (in W m^{-2}, positive upward), **c** Eady growth rate (in 10^{-6} s^{-1}) and **d** storm track activity (in m) on the normalized AMOC time series of the first rotated MCA mode when the ocean leads by 9 years, where the regressions are in phase with the negative NAO-like response in Fig. 4b. The *thick green line* in **a** denotes the climatology of the 20 % sea ice concentration in winter (DJF). The *thick red contours* in **c** and **d** are climatologies with contour interval 5, 6, 7, 8 × 10^{-6} s^{-1} and 2000, 3000, 4000 m respectively. The *thick black contours* in all the *panels* indicate the 90 % confidence level for two-tailed student *t* test

a large similarity between the patterns of the simultaneous AMOC and SLP changes at lag-9 and 0. A positive NAO-like pattern and an anomalous Aleutian low is associated with the enhanced AMOC centered over 50°N at lag-9, while a similar pattern of the opposite sign (spatial pattern correlation of −0.78) is associated with a weakened AMOC. At midlatitude, the amplitude ratio is comparable, as a 60 Pa low over the Azores corresponds to 0.5 Sv AMOC weakening and a 120 Pa high to 1.0 Sv AMOC intensification.

However, the in-phase regression in Fig. 8b may simply reflect the atmospheric forcing of the AMOC, or it may combine atmospheric forcing and response. We use the EFA method (Sect. 2) to effectively separate the atmospheric forcing and response (Frankignoul et al. 1998; Wen et al. 2010). We construct a time series describing the evolution of the SST anomaly pattern in Fig. 7 at lag-9, which is simultaneous with the AMOC intensification in Fig. 8a, by projecting it onto the monthly SST anomaly data in D (December), J (January) and F (February). In order to exclude the sea ice influence, we limit the SST anomaly to south of 55N. We then assess the atmospheric response to this SST anomaly on the monthly time scale using the EFA method. As shown in Fig. 9a, the SLP response resembles the SLP regression on the AMOC index on the interannual time scale (Fig. 8a). It is a positive NAO-like response with an eastward shift, which is most pronounced for its southern lobe, and a weaker anomalous low over the Aleutian region (not significant). There are also some positive SLP anomalies over the Southern Ocean. Hence, the EFA method demonstrates that the SST AMOC fingerprint (the SST anomaly in Fig. 7 at lag-9) indeed generates a NAO-like response in the atmosphere similar to that shown in Fig. 8a.

Note that the in-phase regression of the winter SLP on the monthly SST time series (Fig. 9b) shows large negative anomalies over the Aleutian and a large anticyclone over the North Atlantic resembling an East Atlantic Pattern. This mainly reflects the atmospheric forcing on the SST anomaly (Frankignoul and Hasselmann 1977), and it differs from the SST feedback on the atmosphere (Fig. 9a). In view of the large internal atmospheric variability, the SST anomaly mostly reflects the atmospheric forcing on the ocean at the monthly time scale, while at low frequency, the atmospheric internal variability is largely filtered out and the SST pattern evolution is mostly controlled by the variability of the ocean circulation.

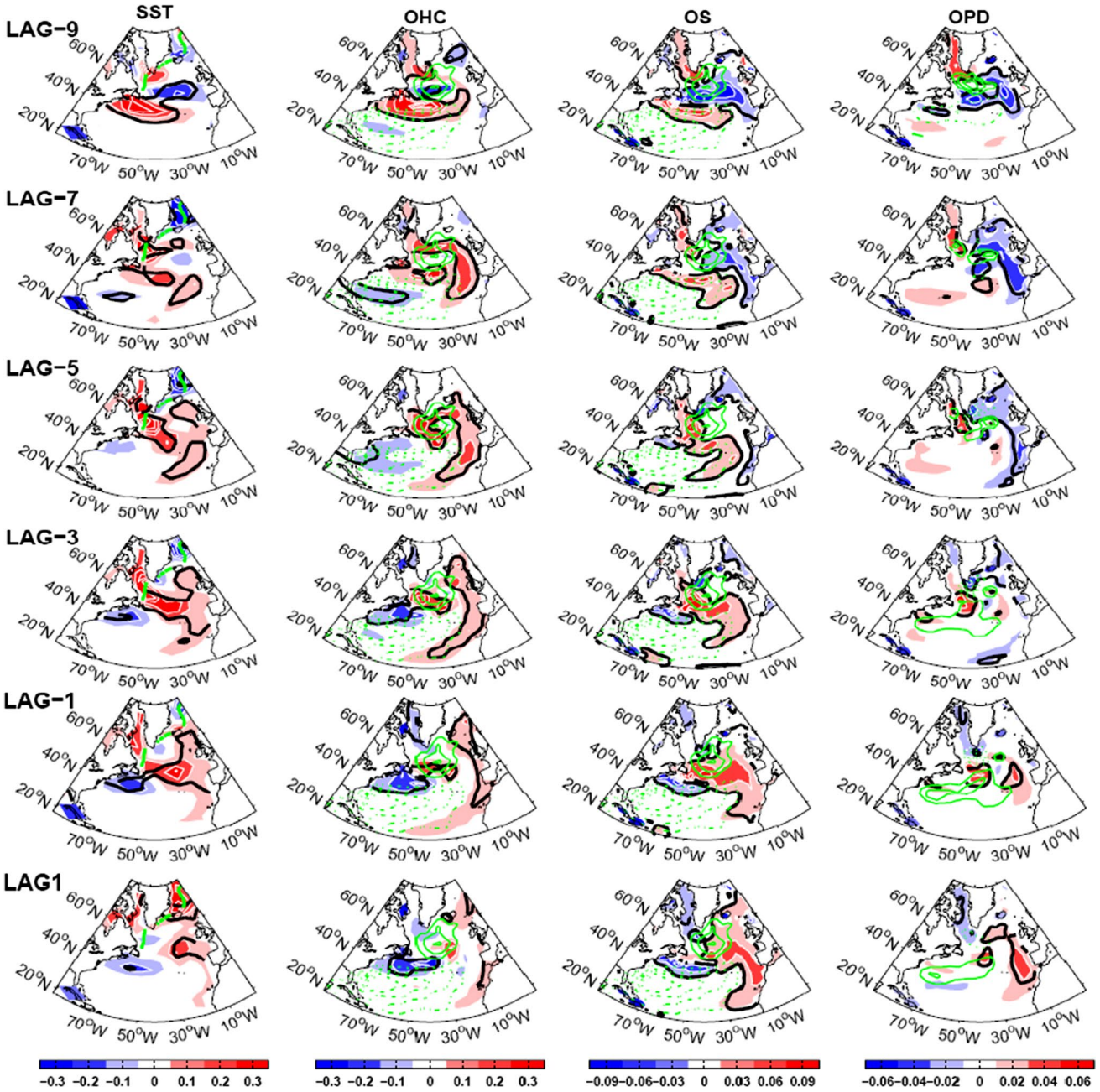

Fig. 7 Regression of winter SST (*left*) and heat content OHC (*middle left*), salinity OS (*middle right*), and potential density OPD (*right*) in the upper 300 m onto the normalized AMOC MCA-time series at lag-9 at different lags, as indicated, where lag-9 is in phase with the positive AMOC in Fig. 4a, and lag 0 would be in phase with the negative NAO-like response in Fig. 4b. The contour interval for the SST, heat content, salinity and potential density is 0.1 K, 10^9 J m^{-2}, 0.03 psu and 0.02 kg m^{-3}, respectively. The *thick black contours* indicate the 90 % confidence level. The *thick green line* in the *left panels* indicates the climatology of the 20 % winter sea ice concentration. The *green contour* in the *middle panels* is the climatological winter barotropic stream function (*solid* for cyclonic flow, contour interval 8 Sv, zero line omitted), while in the *right panels* it shows the lag regression of the winter barotropic stream function (contour interval 0.4 Sv, zero line omitted)

Since the NAO forces the AMOC in the North Atlantic (Fig. 3a) and in turns the AMOC drives a NAO-like signal, there is a positive feedback between the AMOC and the atmosphere, albeit with a slight asymmetry in pattern. According to the MCA in Fig. 3a, the positive NAO forcing enhances the AMOC circulation with a SLP anomaly of about 300 Pa over Azores leading by 1 year a 0.5 Sv AMOC variability. However, this includes the synchronous NAO-like response to the AMOC forcing (Fig. 8), with a 0.5 Sv AMOC change leading to a 60 Pa SLP change, so

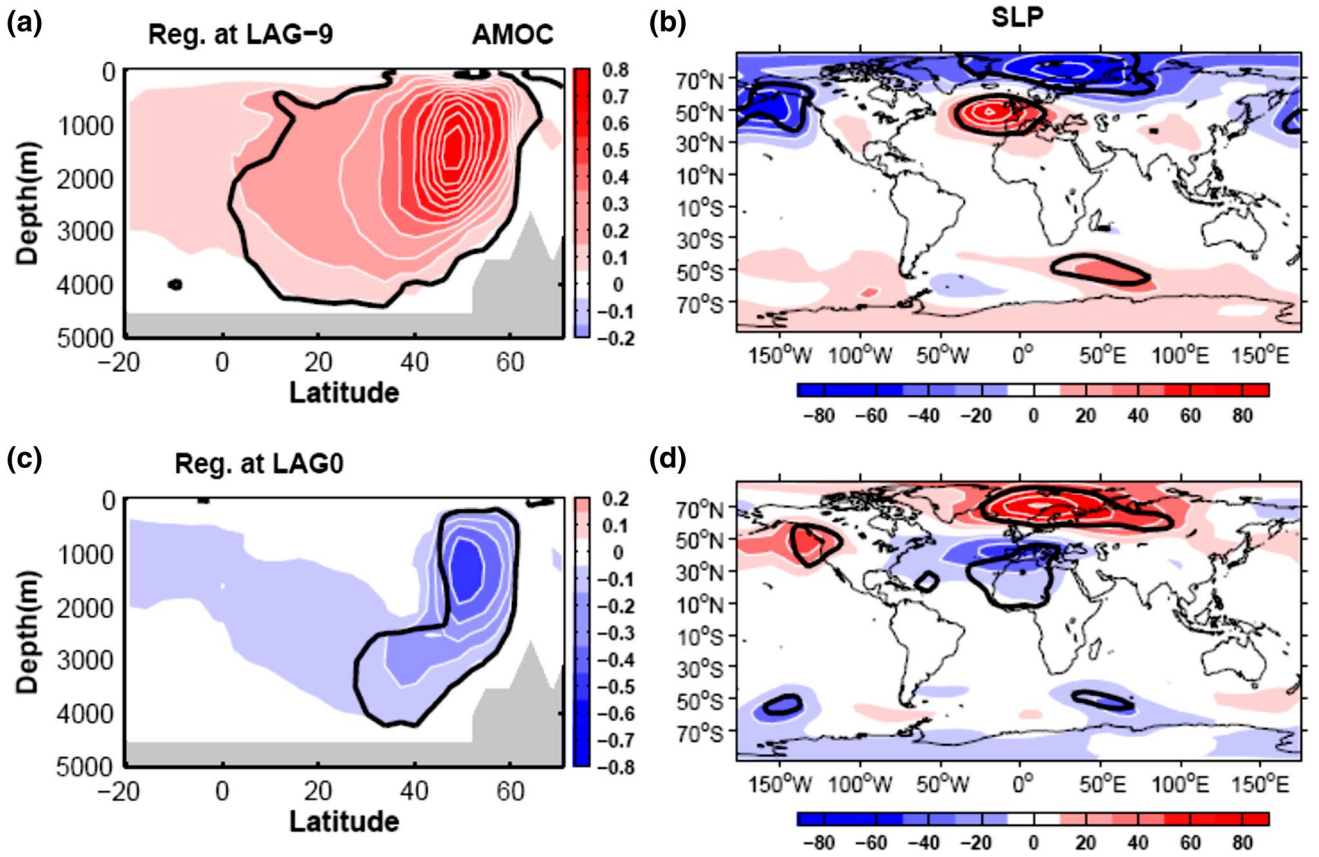

Fig. 8 Regression of the yearly AMOC and winter SLP on the normalized AMOC MCA-time series in Fig. 5a, at lag-9 (**a, b**, in phase with +AMOC in Fig. 4a) and lag 0 (**c**, **d** in phase with the negative NAO-like response in Fig. 4b) respectively. Contour interval is 0.1 Sv for AMOC with positive (negative) for clockwise (anticlockwise) circulation, and 20 Pa for SLP. The thick *black contours* in all the panels indicate the 90 % confidence level for two-tailed student '*t*' test

that the AMOC feedback is about one fourth of the direct atmospheric forcing. This is a notable positive feedback of the AMOC on the atmosphere.

4 Active interaction between AMOC and NAO

The feedback is clearly imprinted in the variability of the atmosphere. The leading mode of winter SLP is the NAO with 43 % of explained variance, and its principal component has a significant autocorrelation at lag of about 10 and 21 years (blue line in Fig. 10), which indicates a robust low frequency variability at the 20-year period. This is close to the oscillatory period of AMOC EOF2, as indicated by the autocorrelation of the AMOC PC2 (black line in Fig. 10), suggesting that the 20 years period of the NAO is the footprint of the AMOC forcing of the atmosphere. This is supported by the cross-correlation between the two PCs (red line in Fig. 10), which shows a significant positive peak when atmosphere leads by 1 or 2 years, and significant negative peaks when ocean leads by 9 years or lags by 11 years. This resembles the MCA result in Fig. 2a, and is consistent with a strong AMOC forcing of the NAO and the damped oscillatory nature of the AMOC.

To give a clearer picture for the interaction between AMOC and NAO, we used the lag regression of yearly (non-filtered) winter fields onto the NAO, since the NAO is its main driver (Sect. 3). The synchroneous regressions (at lag 0 in Fig. 11) show that the NAO cools the surface ocean in the Labrador Sea and subpolar gyre and warms it in the subtropical gyre, consistent with surface heat flux forcing (Cayan 1992). It also strongly deepens the mixed layer in the main deep convection regions, and therefore drives an intergyre gyre circulation, as shown by the barotropical streamfunction. Corresponding to the positive NAO forcing, the synchroneous AMOC response shows a decrease in high latitude and an increase at midlatitude with anomalous downwelling near 50°N, which reflects the rapid barotropic adjustment to the Ekman pumping as described by Eden and Willebrand (2001). When the NAO leads by 1 year (and more so by 2 years), the subtropical and subpolar gyre strengthen and the AMOC is intensified further

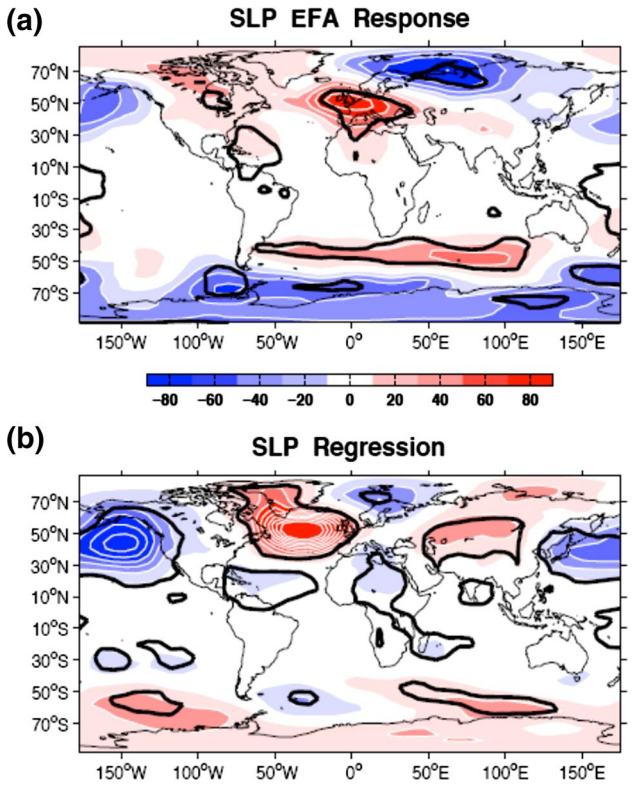

Fig. 9 a The EFA response of the winter SLP (CI = 20 Pa) to the SST anomaly (*upper-left plot* in Fig. 7) on the seasonal time scale. **b** Same as **a**, but for the synchronous regression of the winter SLP (CI = 20 Pa) on the SST anomaly. The *thick black contours* in the *plots* indicate the 90 % confidence level

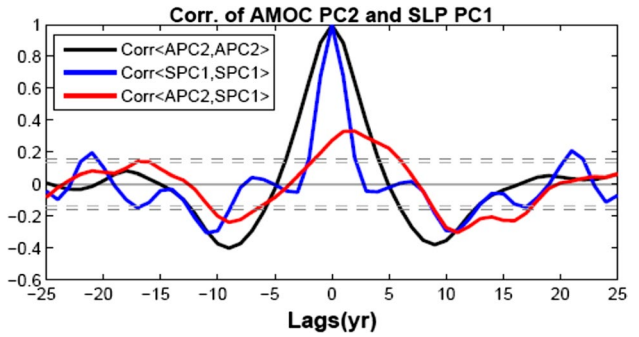

Fig. 10 Autocorrelation of AMOC PC2 (APC2, *black line*) and winter SLP PC1 (SPC1, *blue line*), cross correlation between APC2 and SPC1 (*red line*, SLP leads at positive lag). The *dashed light/dark gray lines* denote the 90 and 95 % confidence level for the cross-correlation respectively, where the sample size is fixed about 245 years for all lead-lag correlations in calculation

north, broadly consistent with the baroclinic adjustment to the NAO-induced buoyancy flux anomaly (e.g. Deshayes and Frankignoul 2008; Yeager and Danabasoglu 2014). As the NAO has no intrinsic year-to-year persistence, the positive NAO-like pattern at lag 1 reflects an ocean influence. The SST anomaly at lag1 is similar to the SST pattern at lag0, but with an enhanced warming in the Gulf Stream region and a weakened cooling in the Labrador Sea, presumably because of advection and reemergence. This NAO-like response at lag 1, is in line with a forcing by the AMOC through its induced SST anomaly. This reflects an active near-synchronous interaction between the AMOC and NAO.

The active coupling between the AMOC and NAO could enhance the low frequency variability of the AMOC on 20-year period. Figure 12 shows the contrast of the AMOC regression on the nomalized SLP PC1 at the large lags when NAO leads and lags. Since the intrinsic NAO memory is limited, the main feature revealed by the regression at lag-9 and lag 11 reflects the AMOC forcing of the atmosphere through its SST fingerprint, with a weakened AMOC generating a negative NAO-like response. However, as a specific comparison, the AMOC variability at positive lags when NAO leads is slight larger than that at the negative lags when there's no atmospheric forcing on the AMOC. It's corresponding to an amplified negative NAO-like response at lag 11, where the center amplitude over the Aleutian is around 80 Pa with the variability enhanced 25 % compared with that of 60 Pa at lag-9. This is probably due to the NAO forcing reinforces the near-synchronous AMOC variability and therefore its following low frequency variability. The contribution of the active air–sea interaction to the low frequency variability of AMOC is further confirmed by the same regression on the NAO index which is get rid of the AMOC signal (proxied by AMOC PC2). It shows a similar result when NAO leads with the moderate reduced amplitude, but a relative large damped signal when NAO lags (not shown). Hence, the near-synchronous coupling of AMOC–NAO plays an active role on the low frequency variability of AMOC, and therefore a robust 20-year period of NAO.

5 Summary and discussion

The winter atmospheric response to the AMOC variability is investigated in the IPSL-CM5A-MR climate model. Using the lagged MCA analysis, a robust atmospheric negative NAO-like response signal was found to follow by 9 years an enhanced AMOC in North Atlantic. The AMOC pattern resembles the second AMOC EOF and has maximum amplitude between 45 and 50°N, and a dominant timescale of 20 year. Correspondingly, the NAO has a small, but significant 20 years variability, suggesting that it responds to the AMOC. The lagged atmosphere signal is established through the AMOC SST fingerprint with cold SST in the Gulf Stream region and warm SST at the downstream near the North Atlantic Current. Through the surface heat flux damping, the dipole pattern SST anomaly changes

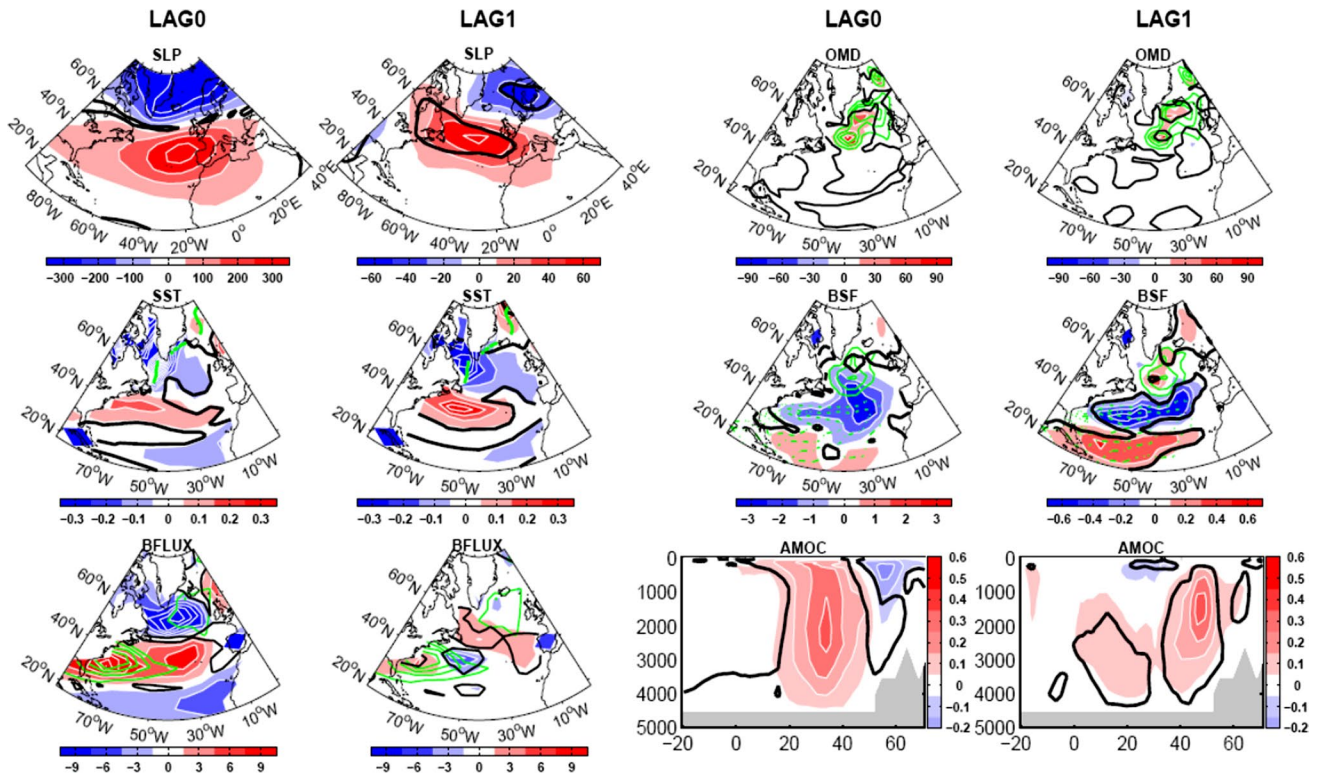

Fig. 11 Regression of the winter SLP (in Pa), SST (in K), buoyancy flux (BFLUX, in 10^{-6} m^2 s^{-3}), ocean mixed-layer depth (OMD, in m), barotropical streamfunction (BSF, in Sv) and the yearly AMOC (in Sv) on the winter SLP EOF PC1 at lag 0 and lag 1 respectively (as Marked on top of the figures), where all the data used are raw data without low pass filter. The contour intervals (CI) are indicated by the *colorbars*. The *green thick contour* in the SST figures indicates the climatology of the 20 % winter sea ice cover. The *green thick contours* in the rest figures are corresponding variables climatology with contour intervals 100, 150, 200, 250 $\times$ 10^{-6} m^2 s^{-3} for buoyancy flux, 200, 400, 600 m for ocean mixed-layer depth and CI = 8 Sv for barotropical streamfunction (solid for cyclonic flow, zero line omitted) respectively. The *black thick contours* in all the figures indicate the 90 % confidence level for two-tailed student '*t*' test

the lower tropospheric baroclinicity and thus the storm track activity, resulting in the negative NAO-like response.

However, we showed that the negative NAO that follows the AMOC intensification actually reflect a fast response to the AMOC weakening that follows it 9 years later, consistent with its 20-year dominant period. The atmospheric response to an enhanced AMOC is thus a positive NAO-like response over the North Atlantic and an anomalous low pressure downstream of the Aleutian region, which is opposite to that detected at 9-year lag by the MCA. Such atmospheric response is confirmed by the EFA method applied to the monthly SST anomaly. Since the NAO drives the AMOC variability, a positive NAO intensifying the AMOC, it indicates a positive feedback between the AMOC and the NAO. The amplitude of the atmospheric response to the AMOC was estimated to be about 1/4 of that of the atmospheric forcing. The active near-synchronous interaction between the AMOC and NAO is further confirmed by the lead-lag relation between AMOC EOF2 and the NAO. It enhances the low frequency variability of AMOC and therefore leads to a robust 20-year period of NAO.

In the IPSL-MR model, one of the robust phenomena is the bi-decadal variability in North Atlantic. This phenomenon has been widely reported in many models (Frankcombe et al. 2010), observations and proxy datas (Banta and McConnell 2007). Several authors (Kwon and Frankignoul 2014; Sévellec and Huch 2015) suggested that the 20–30 years timescale arises from the ocean only, either due to the interaction between the Gulf Stream–North Atlantic Current and the equatorward deep return flow, or to large scale baroclinic instability in the ocean and westward propagation of the subsurface temperature anomalies across the North Atlantic basin, referred as subsurface basin mode (Huck et al. 1999). Sévellec and Fedorov (2013) demonstrated that a damped multidecadal oscillation in the ocean component of the IPSL-CM5A model reflected the latter mechanism. Ortega et al. (2015) further proposed that this mechanism would be coupled in the LR model with surface salinity advection along the subpolar gyre and the atmospheric–seaice interaction in the Nordic Seas (Escudier et al. 2013). They suggested that the two mechanisms play a comparable role in generating the bi-decadal AMOC

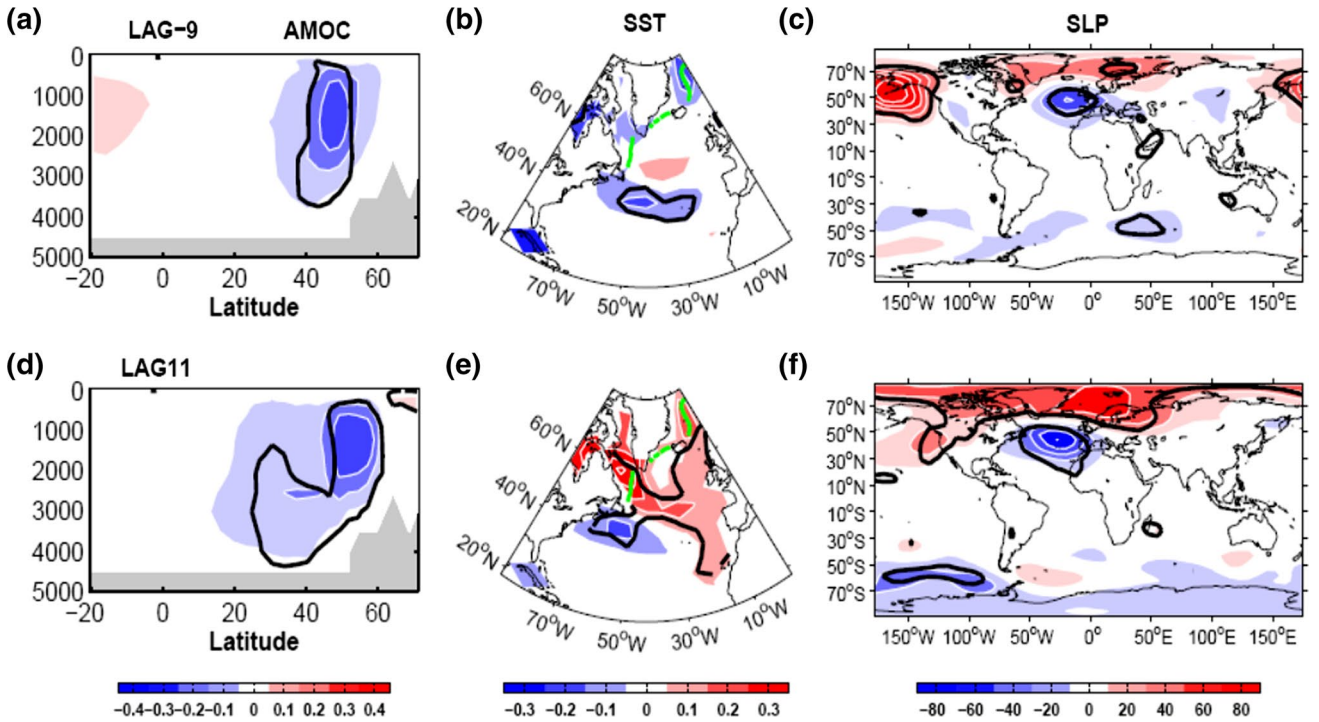

Fig. 12 Lead-lag regression of the yearly AMOC, winter SST and winter SLP on winter SLP PC1 at lag-9 (**a**–**c**) and lag 11 (**d**–**f**), where at lag-9 the ocean is leading by 9 years and at lag 11 it lags by 11 years, respectively. The contour interval for AMOC in the left column is 0.1 Sv with positive (negative) value for anomalous clockwise (counterclockwise), CI = 0.1 K for SST in the middle column and CI = 20 Pa for SLP in the right. The *thick green line* in **d** and **e** denotes the climatology of the 20 % sea ice concentration in winter (DJF). The *black thick contours* in all the *panels* indicate the 90 % confidence level for two-tailed student '*t*' test

variability in North Atlantic. In the IPSL-MR model, there are some similarities in the interplay between the upper ocean advection and westward propagation Rossby wave at depth, which seems to generate the 20-year period of AMOC. However, the specific mechanism is different from that proposed for the LR model (specific investigation for the bi-decadal variability of AMOC in the MR model would be given in a forthcoming paper). Based on our current understanding, the air–sea coupling in the MR model may enhance the low frequency variability of AMOC, but it might not play a substantial role to generate it.

Our results demonstrate that the resolution may modify the coupling of the ocean with the atmosphere. In the IPSL-CM5A LR model, the AMOC-induced SST anomalies are largely located in the subpolar region (GF12, see their Fig. 10). However, in the MR model, the out of phase SST anomaly in the Gulf Stream region seems to also play an active role in the near-synchronous AMOC–NAO interaction. This is presumably because, when the atmospheric resolution is increased, the mean surface wind changes, which may increase the heat flux damping and the baroclinic instability over that region.

The AMOC feedback to the atmosphere and the associated mechanisms may also be model dependent, as a large range of mechanism explain the decadal to multi-decadal AMOC variability in different models (Frankcombe et al. 2008; Liu 2012; MacMartin et al. 2013). Here, we provide a way to understand the interaction between the ocean and the atmosphere, which can be applied to other models. Given the large influence of the coupling illustrated here, our results impel the climate decadal prediction.

Acknowledgments I'd like to thank Drs. Mignot J, Li ZX, Liu ZY and Otega P. for the helpful discussions. We thank the ciclad facility supported by CNRS, UPMC, Labex L-IPSL funded by the ANR (Grant #ANR-10-LABX-0018) and by the European FP7 IS-ENES2 project (Grant #312979). This work is supported by China Scholarship Council (CSC), the European Union 7th Framework Programme (FP7 2007-2013) under Grant Agreement Nos. 308299(NACLIM) and NSFC41475089.

References

Arakelian A, Codron F (2012) Southern hemisphere jet variability in the IPSL GCM at varying resolutions. J Atmos Sci 69(12):3788–3799

Banta JR, McConnell JR (2007) Annual accumulation over recent centuries at four sites in central Greenland. J Geophys Res. doi:10.1029/2006JD007887

Barnes EA, Polvani L (2013) Response of the midlatitude jets, and of their variability, to increased greenhouse gases in the CMIP5 models. J Clim 26(18):7117–7135
Booth BB, Dunstone NJ, Halloran PR et al (2012) Aerosols implicated as a prime driver of twentieth-century North Atlantic climate variability. Nature 484:228–232
Bretherton CS, Smith C, Wallace JM (1992) An intercomparison of methods for finding coupled patterns in climate data. J Clim 5:541–560
Cayan DY (1992) Latent and sensible heat flux anomalies over the northern oceans: driving the sea surface temperature. J Phys Oceanogr 22:859–881
Cheng X, Dunkerton TJ (1995) Orthogonal rotation of spatial patterns derived from singular value decomposition analysis. J Clim 8:2631–2643
Czaja A, Frankignoul C (2002) Observed impact of Atlantic SST anomalies on the North Atlantic oscillation. J Clim 15:606–623
Delworth TL, Greatbatch RJ (2000) Multidecadal thermohaline circulation variability driven by atmospheric surface flux forcing. J Clim 13:1481–1495
Deser C, Tomas RA, Peng SL (2007) The transient atmospheric circulation response to North Atlantic SST and sea ice anomalies. Clim Dyn 20:4751–4767
Deshayes J, Frankignoul C (2008) Simulated variability of the circulation in the North Atlantic from 1953 to 2003. J Clim 21:4919–4933
Dong B, Sutton RT (2005) Mechanism of interdecadal thermohaline circulation variability in a coupled ocean–atmosphere GCM. J Clim 18:1117–1135
Dufresne J, Foujols S, Denvil S et al (2013) Climate change projections using the IPSL-CM5 earth system model: from CMIP3 to CMIP5. Clim Dyn 40:2123–2165
Eden C, Willebrand J (2001) Mechanism of interannual to decadal variability of the North Atlantic circulation. J Clim 14:2266–2280
Escudier R, Mignot J, Swingedouw D (2013) A 20-year coupled ocean-seaice-atmosphere variability mode in the North Atlantic in an AOGCM. Clim Dyn 40:619–636
Farneti R, Vallis GK (2009) Mechanisms of interdecadal climate variability and the role of ocean–atmosphere coupling. Clim Dyn. doi:10.1007/s00382-009-0674-9
Frankcombe L, Dijsktra HA, von der Heydt A (2008) Sub-surface signatures of the Atlantic Multidecadal Oscillation. Res. Lett, Geophys. doi:10.1029/2008GL034989
Frankcombe L, von der Heydt A, Dijsktra HA (2010) North Atlantic multidecadal climate variability: an investigation of dominant time scales and processes. J Clim 23:3626–3638
Frankignoul C, Hasselmann K (1977) Stochastic climate models, part II application to sea-surface temperature anomalies and thermocline variability. Tellus 29(4):289–305
Frankignoul C, Kestenare E (2002) The surface heat flux feedback. Part I: estimates from observations in the Atlantic and the North Pacific. Clim Dyn 19:633–647
Frankignoul C, Czaja A, Heveder B (1998) Air–sea feedback in the North Atlantic and surface boundary conditions for ocean models. J Clim 11:2310–2324
Frankignoul C, Gastineau G, Know YO (2013) The influence of the AMOC variability on the atmosphere in CCSM3. J Clim 26:9774–9790
Ganachaud A, Wunsch C (2003) Large-scale ocean heat and freshwater transports during the World Ocean Circulation Experiment. J Clim 16:696–705
Gastineau G, Frankignoul C (2012) Cold-season atmospheric response to the natural variability of the Atlantic meridional overturning circulation. Clim Dyn 39:37–57
Gastineau G, Frankignoul C (2015) Influence of the North Atlantic SST variability on the atmospheric circulation during the twentieth-century. J Clim, Accepted
Hodson D, Sutton R, Cassou C et al (2010) Climate impacts of recent multidecadal changes in Atlantic Ocean sea surface temperature: a multimodel comparison. Clim Dyn 34:1041–1058
Hoskins B, Valdes P (1990) On the existence of storm tracks. J Atmos Sci 47:1854–1864
Huck T, Verdiere AC, Weaver AJ (1999) Interdecadal variability of the thermohaline circulation in box-ocean models forced by fixed surface fluxes. J Phys Oceanogr 29:865–892
Johns W et al (2011) Continuous, array-based estimates of the Atlantic Ocean heat transport at 26.5N. J Clim 24:2429–2449
Jungclaus J, Haak H, Latif M et al (2005) Arctic-North Atlantic interactions and multi-decadal variability of the meridional overturning circulation. J Clim 18:4013–4031
Knight J, Allan R, Folland C et al (2005) A signature of persistent natural thermohaline circulations in observed climate. Geophys Res Lett 32:L20708. doi:10.1029/2005GL024233
Kwon Y, Frankignoul C (2014) Mechanisms of multidecadal Atlantic meridional overturning circulation variability diagnosed in depth versus density space. J Clim 27(24):9359–9376
Latif M, Roeckner E, Botzet M et al (2004) Reconstructing, monitoring and predicting multidecadal-scale changes in the North Atlantic thermohaline circulation with the sea surface temperature. J Clim 17:1605–1614
Liu Z (2012) Dynamics of interdecadal climate variability: a historical perspective. J Clim 25:1963–1995
MacMartin D, Tziperman E, Zanna L (2013) Frequency domain multimodel analysis of the response of atlantic meridional overturning circulation to surface forcing. J Clim 26(21):8323–8340
Marini C, Frankignoul C (2013) An attempt to deconstruct the Atlantic multidecadal oscillation. Clim Dyn 43:607–625. doi:10.1007/s00382-013-1852-3
McCarthy G, Frajka-Williams E, Johns WE, Baringer MO et al (2012) Observed interannual variability of the Atlantic meridional overturning circulation at 26.5N. Geophys Res Lett. doi:10.1029/2012GL052933
Mignot J, Ganopolski A, Levermann A (2007) Atlantic subsurface temperature: response to a shutdown of the overturning circulation and consequences for its recovery. J Clim 20:4884–4898
Msadek R, Frankignoul C (2009) Atlantic multidecadal oceanic variability and its influence on the atmosphere in a climate model. Clim Dyn 33:45–62
Ortega P, Mignot J, Swingedouw D, et al. (2015) Reconciling two alternative mechanisms behind bi-decadal variability in the North Atlantic. Prog Oceanogr 137:237–249
Ottera OH, Bentsen M, Drange H, Suo L (2010) External forcing as a metronome for Atlantic multidecadal variability. Nat Geosci 3:688–694
Pohlmann H, Sienz F, Latif M (2006) Influence of the multidecadal Atlantic meridional overturning circulation variability on European climate. J Clim 19:6062–6067
Rayner D et al (2011) Monitoring the Atlantic meridional overturning circulation. J Clim 58:1744–1753
Rodwell DP, Folland CK, Maskell K, Ward MN (1995) Variability of summer rainfall over tropical north Africa (1906–92): observations and modeling. Q J R Meterorol Soc 121:669–704
Sévellec F, Fedorov A (2013) The leading, interdecadal eigenmode of the Atlantic meridional overturning circulation in a realistic ocean model. J Clim 26(7):2160–2183
Sévellec F, Huch T (2015) Theoretical investigation of the Atlantic multidecadal oscillation. J Phys Oceanogr 45(9):150413133522004. doi: 10.1175/JPO-D-14-0094.1
Sutton RW, Hodson DLR (2005) Atlantic ocean forcing of North American and European summer climate. Science 309:115–118
Teng H, Branstator G, Meehl G (2011) Predictability of the Atlantic overturning circulation and its associated surface patterns

in two CCSM3 climate change ensemble experiments. J Clim 24:6054–6076

Timmermann A, Latif M, Voss R et al (1998) Northern hemispheric interdecadal variability: a coupled air–sea mode. J Clim 11:1906–1931

Ting M, Kushnir Y, Li C (2014) North Atlantic Multidecadal SST Oscillation: external forcing versus internal variability. J Mar Syst 133:27–38

Vellinga M, Wu P (2004) Low-latitude freshwater influence on centennial variability of the Atlantic thermohaline circulation. J Clim 17:4498–4511

Wen N, Liu Z, Liu Q, Frankignoul C (2010) Observed atmospheric responses to global SST variability modes: a unified assessment using GEFA. J Clim 23:1739–1759

Yeager S, Danabasoglu G (2014) The origins of late-twentieth-century variations in the large-scale North Atlantic circulation. J Clim 27:3222–3246

Yeager S, Karspeck A, Danabasoglu G et al (2012) A decadal prediction case study: late twentieth-centrury North Atlantic Ocean heat content. J Clim 25:5173–5189